INTERNATIONAL JOURNAL FOR NUMERICAL METHODS IN FLUIDS, VOL. 8, 327–338 (1988)

THE NUMERICAL SOLUTION OF STOKES FLOW IN A DOMAIN WITH RE-ENTRANT BOUNDARIES BY THE BOUNDARY ELEMENT METHOD

A. K. MITRA AND M. S. INGBER

Department of Engineering Science and Mechanics, Iowa State University, Ames, Iowa, 50011, U.S.A.

SUMMARY

Numerical solutions are presented for two-dimensional low Reynolds number flow in a rotating tank with stationary barriers. The boundary element method is employed, assuming straight panels and quadratic source distribution. The feasibility of repositioning the nodes as a way to minimize the error is explored. A stretching parameter places smaller elements near the re-entrant regions. Elementary error analysis shows uniform improvement in the solution with stretching. The changing eddy pattern for different numbers and sizes of the barriers is compared with experimental results.

KEY WORDS Boundary element method Stokes flow Re-entrant boundaries

INTRODUCTION

The Navier–Stokes equations can be linearized in those fortuitous circumstances where the Reynolds number is very low. However, in many problems of engineering interest (for example, in lubrication) the solution of the linearized equations is not simple because of the complex geometry involved. In these situations the resulting biharmonic equation can be conveniently solved by the boundary element method (BEM).[1–4] The advantages of the BEM are that the interior of the domain need not be discretized and discretization of a boundary of complex shape poses no additional difficulty. However, the discretization of the boundary requires special care when sharp corners are present on the boundary or the boundary conditions are discontinuous. Either of these would introduce a mathematical singularity in the vorticity.[4,5] The presence of these singularities is detrimental to the quality of the solution. The quality of the BEM solution can be improved by inserting the proper singularity analytically and solving only the regular part numerically.[4–6]

In this paper an attempt is made to improve the BEM solution by refining the grid near the singularities. The principle of grid refinement is based on some observations concerning the finite element method (FEM). It has been found[7] that the accuracy and convergence of the FEM depend on the smoothness of the solution, where the smoothness indicates how many square integrable derivatives the solution has. Extending this idea to the BEM, we plan to refine the grid selectively near the singularities of the vorticity where the stream function is less smooth. The refinement could be achieved by the introduction of additional nodes or by an optimum arrangement of a fixed number of nodes. Here the second approach is used, where a higher accuracy is obtained by the same amount of computation. The process of reaching the optimum is iterative. At each stage the error in the solution is gauged and the changes are introduced accordingly. The BEM has a distinct

0271–2091/88/030327–12$06.00

Received 1 December 1986
Revised 24 April 1987

advantage over the FEM in gauging the error in the solution. Since the numerical solution in the BEM is expressed as integrals involving the suitable Green's function, it satisfies the governing equation exactly within the domain; a comparison of the numerical solution with the specified conditions on the boundary provides an error measure. In other words, the more rigidly we enforce the boundary conditions, the closer we get to the exact solution.

For demonstration purposes we consider the low Reynolds number flow of an incompressible fluid in a rotating tank with stationary barriers. This problem exemplifies certain computational difficulties associated with solving the biharmonic equation in domains of complex geometry. The fluid turns around sharp edges and corners and shows a changing eddy pattern when the height of the barriers is changed. The nature of the flow field has been found experimentally[8] to be sensitive to the geometry; that is, small changes in the height of the barriers can dramatically alter the nature of the entire flow field. This sensitivity demands that errors accrued near the re-entrant regions and in the corners where the boundary conditions are discontinuous should be monitored carefully. In certain cases the integrity of the numerical solution can be impaired if these errors are not minimized. The method of grid repositioning, in which the size of the elements is reduced in regions of large error, is shown to be an effective method not only of reducing errors in the corners and re-entrant regions but also of achieving global reductions in the error.

MODEL PROBLEM

As the model problem, consider the case with four tabs (barriers) as shown in Figure 1. The rotating tank is designated as the boundary Γ_1 and the four tabs are designated as the boundary Γ_2.

The governing equations can be written in terms of a suitably non-dimensionalized stream function ψ as

$$\nabla^4 \psi(x, y) = 0 \quad \text{in} \quad \Omega, \tag{1}$$

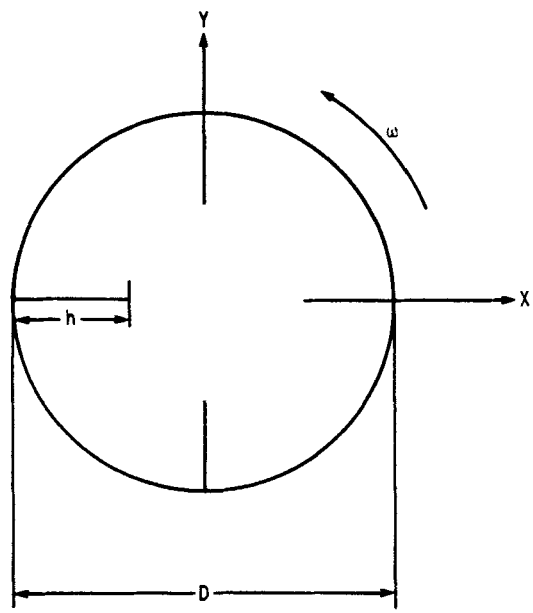

Figure 1. Problem geometry

with the boundary conditions

$$\begin{aligned} &\psi(x,y)=0 \quad \text{on} \quad \Gamma_1+\Gamma_2,\\ &\frac{\partial\psi}{\partial n}(x,y)=-1 \quad \text{on} \quad \Gamma_1,\\ &\frac{\partial\psi}{\partial n}(x,y)=0 \quad \text{on} \quad \Gamma_2, \end{aligned} \tag{2}$$

where n is the co-ordinate along the unit outward normal $\mathbf{n}$ to the boundary of domain Ω.

Two categories of boundary element formulation can be found in the literature: the direct formulation[2,4] and the indirect formulation.[1,3] Here the second approach is taken and the solution of equation (1) is written as

$$\psi(\mathbf{p})=r^2\phi(\mathbf{p})+\theta(\mathbf{p}), \tag{3}$$

where ϕ and θ are harmonic functions, $\mathbf{p}=(x,y)$ is a point in the domain and $r^2=x^2+y^2$. The functions ϕ and θ may be expressed as boundary integrals representing simple source distributions along $\partial\Omega=\Gamma_1+\Gamma_2$. That is, if $\mathbf{q}$ is a point on the boundary $\partial\Omega$ and s is the parameter of arc length along the boundary, then

$$\phi(\mathbf{p})=\int_{\partial\Omega} G(\mathbf{p},\mathbf{q})\sigma(\mathbf{q})\,ds(\mathbf{q}), \tag{4}$$

$$\theta(\mathbf{p})=\int_{\partial\Omega} G(\mathbf{p},\mathbf{q})\rho(\mathbf{q})\,ds(\mathbf{q}), \tag{5}$$

where

$$G(\mathbf{p},\mathbf{q})=\ln|\mathbf{p}-\mathbf{q}|. \tag{6}$$

Inserting equations (3)–(5) into equations (2) yields the following integral equations for the source strengths $\sigma(\mathbf{q})$ and $\rho(\mathbf{q})$:

$$|\mathbf{p}|^2\int_{\partial\Omega} G(\mathbf{p},\mathbf{q})\sigma(\mathbf{q})\,ds(\mathbf{q})+\int_{\partial\Omega} G(\mathbf{p},\mathbf{q})\rho(\mathbf{q})\,ds(\mathbf{q})=0, \quad \mathbf{p}\in\partial\Omega, \tag{7}$$

$$\begin{aligned} &|\mathbf{p}|^2\int_{\partial\Omega} G'(\mathbf{p},\mathbf{q})\sigma(\mathbf{q})\,ds(\mathbf{q})+(|\mathbf{p}|^2)'\int_{\partial\Omega} G(\mathbf{p},\mathbf{q})\sigma(\mathbf{q})\,ds(\mathbf{q})\\ &\quad+\int_{\partial\Omega} G'(\mathbf{p},\mathbf{q})\rho(\mathbf{q})\,ds(\mathbf{q})=f(\mathbf{p}), \quad \mathbf{p}\in\partial\Omega, \end{aligned} \tag{8}$$

where

$$f(\mathbf{p})=\begin{cases} -1, & \mathbf{p}\in\Gamma_1,\\ 0, & \mathbf{p}\in\Gamma_2. \end{cases} \tag{9}$$

The prime on G denotes the derivative along the outward normal to the boundary at the point $\mathbf{p}$.

NUMERICAL SOLUTION

In order to solve equations (7)–(9) for $\sigma(\mathbf{q})$ and $\rho(\mathbf{q})$, the boundary $\partial\Omega$ is approximated by N straight boundary elements (panels). Then the integrals in equations (7) and (8) become

$$\sum_{j=1}^{N} \int_{\partial\Omega_j} G(\mathbf{p}, \mathbf{q}_j)\sigma_j(\mathbf{q}_j)\,\mathrm{d}s(\mathbf{q}_j), \tag{10}$$

$$\sum_{j=1}^{N} \int_{\partial\Omega_j} G'(\mathbf{p}, \mathbf{q}_j)\sigma_j(\mathbf{q}_j)\,\mathrm{d}s(\mathbf{q}_j), \tag{11}$$

with similar expressions containing $\rho_j(\mathbf{q}_j)$, where $\partial\Omega_j$ represents the jth panel. If the variations of σ_j and ρ_j are assumed quadratic on each panel, then they can be expressed in terms of appropriate shape functions[9] and values of σ_j and ρ_j at three points on the panel; that is,

$$\sigma_j(\mathbf{q}_j) = \sum_{i=1}^{3} S_i(\mathbf{q}_j)\sigma_{ij}, \tag{12}$$

$$\rho_j(\mathbf{q}_j) = \sum_{i=1}^{3} S_i(\mathbf{q}_j)\rho_{ij}. \tag{13}$$

The general form of the shape function is

$$S_i(\mathbf{q}_j) = \sum_{m=0}^{2} C_{mi} q_j^m, \tag{14}$$

where C_{mi} are known constants. The stream function and its derivative along the outward normal at a collocation point $\mathbf{p}_k$ on the boundary can now be written as

$$\psi(\mathbf{p}_k) = |\mathbf{p}_k|^2 \sum_{j=1}^{N} \sum_{i=1}^{3} \sigma_{ij} U_{kij} + \sum_{j=1}^{N} \sum_{i=1}^{3} \rho_{ij} U_{kij} = 0, \tag{15}$$

$$\psi'(\mathbf{p}_k) = (|\mathbf{p}_k|^2)' \sum_{j=1}^{N} \sum_{i=1}^{3} \sigma_{ij} U_{kij} + |\mathbf{p}_k|^2 \sum_{j=1}^{N} \sum_{i=1}^{3} \sigma_{ij} V_{kij} + \sum_{j=1}^{N} \sum_{i=1}^{3} \rho_{ij} V_{kij} = f(\mathbf{p}_k), \tag{16}$$

where

$$U_{kij} = \int_{\partial\Omega_j} G(\mathbf{p}_k, \mathbf{q}_j) S_i(\mathbf{q}_j)\,\mathrm{d}s(\mathbf{q}_j), \tag{17}$$

$$V_{kij} = \int_{\partial\Omega_j} G'(\mathbf{p}_k, \mathbf{q}_j) S_i(\mathbf{q}_j)\,\mathrm{d}s(\mathbf{q}_j). \tag{18}$$

The ultimate unknowns are then the source strengths σ_{ij} and ρ_{ij}. If there are $2M$ unknowns, then these are solved by writing equations (15) and (16) at M collocation points. On each panel the two end points and the midpoint are taken as the collocation and the source points.

The integrations can be carried out numerically[9] or analytically.[10,11] In the present study analytical integration is possible because straight panels have been chosen, and analytical integration is computationally economical because it was found that the logarithmic kernel requires smaller subdivisions for numerical integration when the field point is close to the source panel. Since published expressions[10] for the six integrals involved in U_{kij} and V_{kij} have typographical errors, they have been included in the Appendix.

ERROR ANALYSIS

If a norm is defined as

$$\|\psi\|_{1,\Omega} = \left(\int_{\Omega} |\psi|^2\,\mathrm{d}\Omega + \int_{\Omega} \left|\frac{\partial\psi}{\partial x}\right|^2 \mathrm{d}\Omega + \int_{\Omega} \left|\frac{\partial\psi}{\partial y}\right|^2 \mathrm{d}\Omega \right)^{1/2}, \tag{19}$$

then the boundary element error can be expressed as

$$E(\psi, \psi_h, \mathbf{h}) = : \|\psi - \psi_h\|_{1,\Omega}, \tag{20}$$

where ψ represents the exact solution, ψ_h the boundary element solution, and $\mathbf{h} = (h_1, h_2, \ldots, h_k)$ represents the partitioning of the boundary defined by the element lengths. Since ψ is unknown within Ω, a second error norm is defined in terms of specified boundary data:

$$EB(\psi, \psi_h, \mathbf{h}) = : \|\psi - \psi_h\|_{1,\Gamma}, \tag{21}$$

where

$$\|\psi\|_{1,\Gamma} = \left(\int_\Gamma |\psi|^2 \, d\Gamma + \int_\Gamma \left| \frac{\partial \psi}{\partial n} \right|^2 d\Gamma \right)^{1/2}. \tag{22}$$

It is shown by Ingber and Mitra[12] that

$$E(\psi, \psi_h, \mathbf{h}) \leqslant CEB(\psi, \psi_h, \mathbf{h}), \tag{23}$$

where C is a constant independent of the discretization. Thus minimizing the error in the boundary norm (EB) will provide the best bound on the error in the entire domain. Since the boundary error norm is a measurable quantity, it can be minimized through numerical experiments by changing the size of the elements. Ingber and Mitra suggested a method for automatic optimization of the discretization.[12] In this paper the results of the numerical experiments mentioned above are given. Re-discretization is not an arbitrary procedure. The error norm for each panel provides clues for this process, especially for a boundary with sharp edges and corners or where the specified boundary data has discontinuities.

In the present problem the error norm EB was found to be much larger than average for panels near the re-entrant edges and the corners where the tank meets the tabs. Rapid changes in the dependent variable near singularities resulted in oscillatory solutions for the source strengths, giving rise to large errors in these regions. Problems of this nature have been previously investigated by Bernal and Whiteman[6] and Kelmanson.[5] These investigators combined an analytic representation of the singularity with their numerical methods. Additional collocation points were incorporated to determine the additional unknown constants associated with the analytical singular parts. The present approach is perhaps more general in that it is not dependent on the nature of the singularity and will also work for boundaries that approximate corners or re-entrant regions, such as the leading edge of a thin aerofoil.

In the present method, when a large boundary error is observed in a region, the boundary conditions are enforced more rigidly by employing smaller elements in that region while maintaining the same total number of elements. This has been done by using a stretching parameter ($S < 1$). The largest elements are placed near the centre of the barrier or the tank in each sector. The sizes of the elements are shortened, using the stretching parameter, according to a geometric progression as a corner or edge is approached.

OPTIMIZATION

In Figure 2 the discretization with stretching (S_1 on tank and S_2 on barrier) for the top half of the tank with two barriers is shown. The stretching on the tank and barriers can be independently selected. The optimization process has been started with both stretchings being at unity. Only the stretching on the tab was then reduced until a minimum in the error norm was found. Keeping the stretching on the tab constant at the value corresponding to this minimum, the stretching on the tank was reduced. The process was continued until a 'global minimum' was reached. The

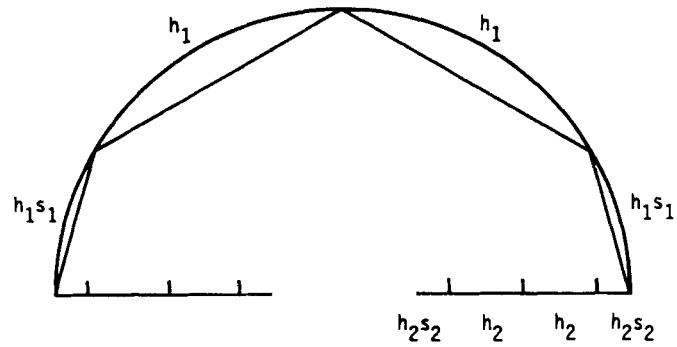

Figure 2. Use of stretching parameters for two barriers

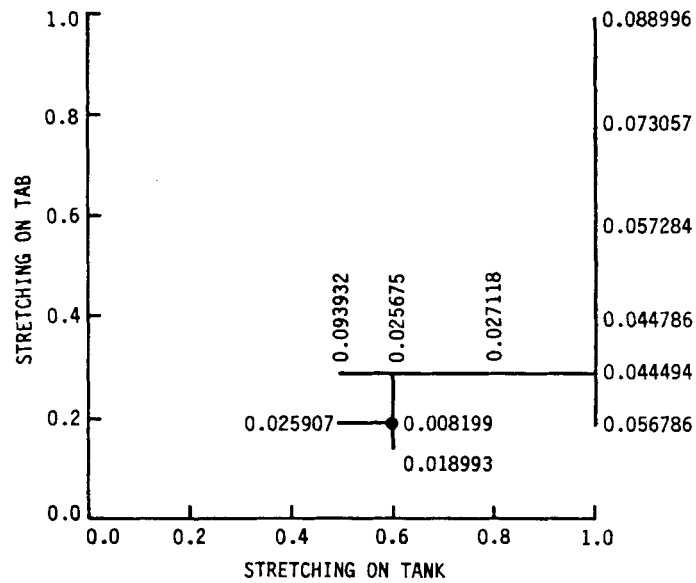

Figure 3. Optimization for two barriers with $h/D = 0{\cdot}2$

results of this optimization process are presented for one case with two barriers where the barrier height non-dimensionalized by the tank diameter is 0·2. Each half of the tank is divided into 16 panels, and six panels are placed on each barrier. The path leading to the 'optimum' is shown in Figure 3 together with the value of EB for several stretching combinations. However, the optimum is restricted to the chosen goemetric progression for the size of the elements. Though more general variation in size may provide a better solution, the basic advantages of the method can be seen quantitatively. The error norm has been calculated for each panel and then squared and summed to get the total error. For each panel the norm was calculated by a one-point integration formula using the error at a point halfway between two collocation points where the error is expected to be maximum. The zigzag path leading to the optimum suggests that the optimum is related non-linearly with the two stretchings. However, independent variation of the stretchings leads to the correct end result. In Figures 4 and 5 the error in the Neumann condition on each panel is plotted for the uniform as well as the optimum discretization. The curved boundary is straightened out for convenience in plotting. When shorter elements were

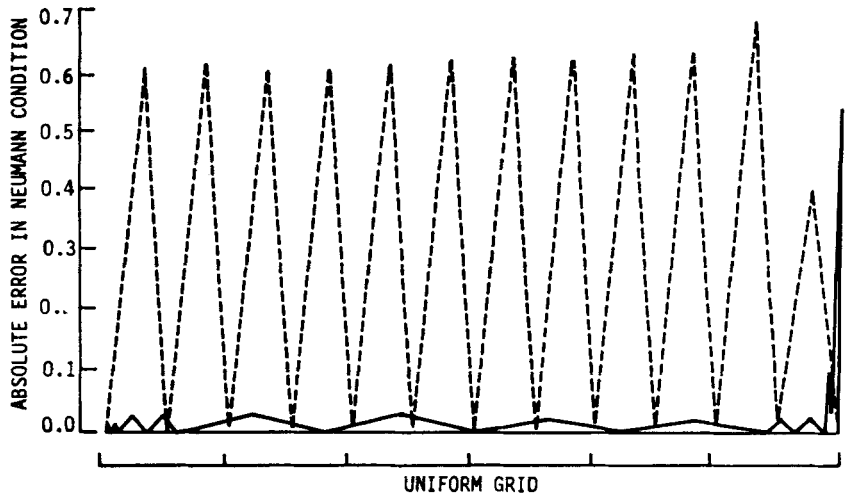

Figure 4. Error in Neumann condition on a barrier

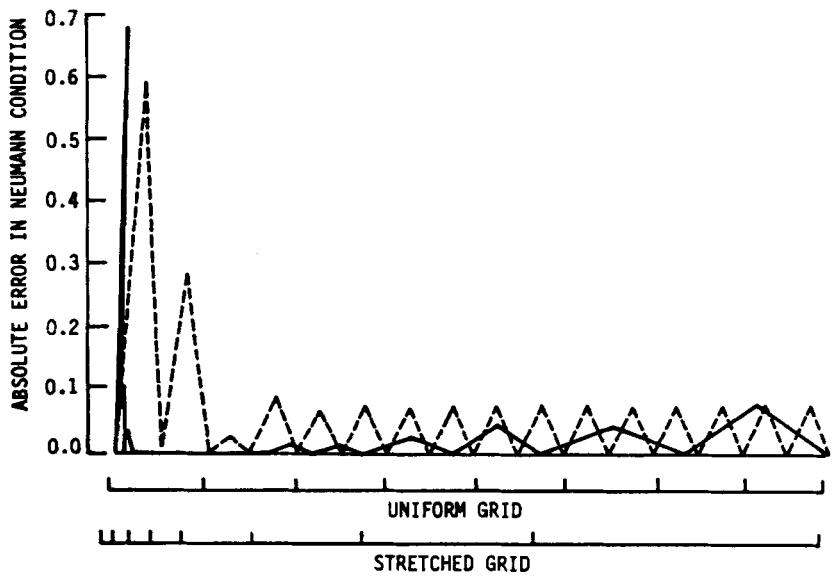

Figure 5. Error in Neumann condition on the tank

placed near the edges, the lengths of elements elsewhere were made larger in order to keep the total number of elements fixed. Even so, the error plot shows a uniform reduction in error spikes. The sharp error spikes near the corner (within a circle of radius 0·01 centred at the corner) where the tank meets the barrier appear for two reasons. First the boundary conditions are inconsistent 'at' the corner, because the corner belongs to the stationary barrier as well as the moving tank. The second reason, which is purely procedural, is that the direction of the normal to the surface cannot be correctly specified at this point. Kelmanson[5] has given the nature of the stream function near such corners but has not shown how the Neumann error improved when the analytical nature of the solution is built into the numerical solution. However, the value of the function itself converged quickly through Kelmanson's modification.[5] Similar improvements have been observed through

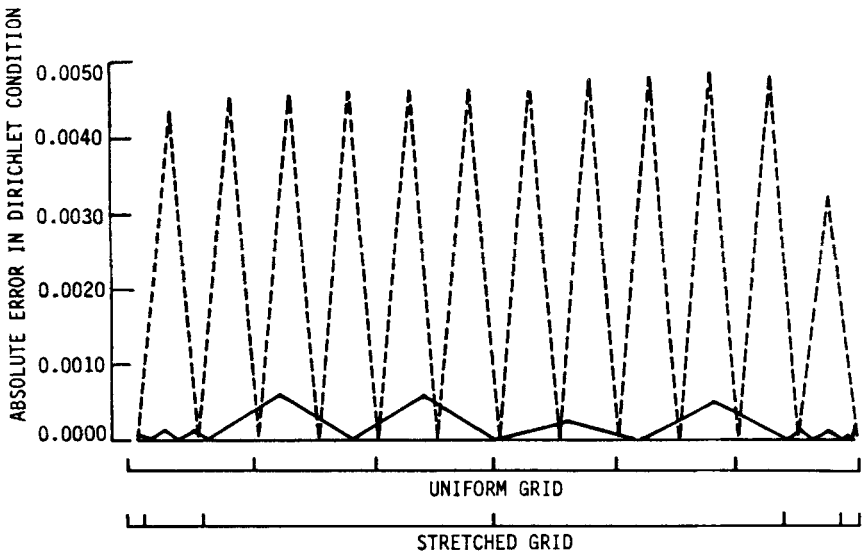

Figure 6. Error in Dirichlet condition on a barrier

stretching, as shown in Figure 6 where the value of the stream function (Dirichlet error) is plotted along the barrier.

As the stretching parameter is reduced, the condition number of the coefficient matrix increases. In all cases presented in this paper the condition number has always been less than 10^5. For a condition number of this order, double-precision arithmetic is essential.

The efficiency of the optimization process can be demonstrated by a comparison of computation costs between uniform grids having a large number of elements and the optimal grid. For the example case of the tank with two barriers and $h/D = 0{\cdot}2$, in which half of the tank is divided into 16 panels and the tab is divided into six panels, each iteration took 9 CPU seconds on a VAX/VMS system. As shown in Figure 3, 12 iterations were needed to obtain the optimal grid, and therefore a total of 108 CPU seconds were expended. The resulting boundary error for the optimal grid was given by $EB = 0{\cdot}019$ (see equation (21)). By using a uniform grid but increasing the number of panels on the tank and tab proportionally, it was determined for a discretization with 80 panels per half-tank and 30 panels per tab that a total of 712 CPU seconds were expended, resulting in a boundary error $EB = 0{\cdot}174$. It is thus clear that the optimal grid far outperforms the uniform grid in terms of cost and accuracy.

RESULTS

The improvement in the interior that can be achieved by stretching is shown quantitatively in Figure 7. The location of the stagnation point in a tank with two barriers is plotted against the barrier height. The details of the grid are given in Table I. When the height of the barrier is small, $h/D = 0{\cdot}1$, the solution with a uniform grid does not show any stagnation point. The stagnation point can only by resolved by optimizing the element lengths. When the height of the barrier is increased, the flow becomes compartmentalized in the two halves of the tank. Though the singularity continues to exist at the sharp edge, its effect gets diminished. As a result the optimization process loses it significance. For $h/D = 0{\cdot}3$ and $h/D = 0{\cdot}4$ the results for uniform and optimum grids are almost identical.

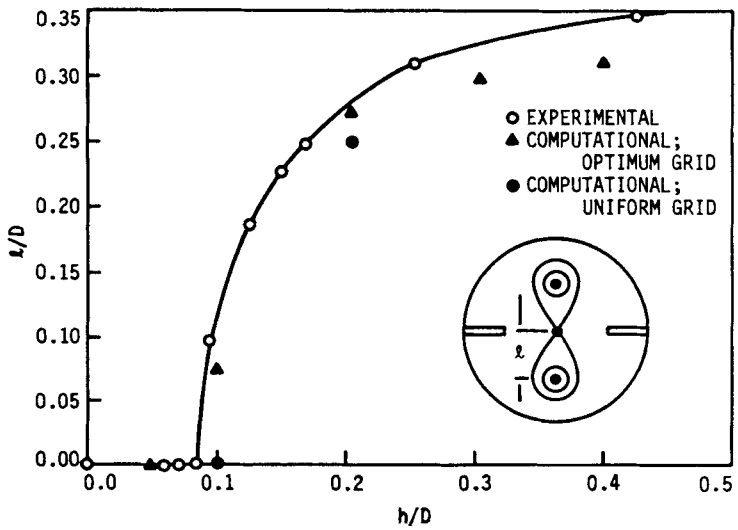

Figure 7. Stagnation point separation distance as a function of barrier height

Table 1

Barriers	h/D	Panels/barrier	Panels/sector of tank	S_1	S_2
2	0·1	6	24	1·0	0·05
	0·2	12	24	1·0	0·3
	0·3	18	24	1·0	0·45
	0·4	24	24	1·0	0·55
4	0·2	6	6	1·0	0·3
	0·25	6	6	1·0	0·2
	0·3	6	6	1·0	0·2

The stream function for several cases with four barriers is also determined. In all the cases the optimum stretching combination (see Table I) was found. The flow with one central stagnation point is shown in Figure 8(a); in Figure 8(b) the flow has one central and four outer stagnation points. All five eddies rotate in the same direction as the tank. No effort has been made to identify the conspicuous case of five central stagnation points coalescing into one, as is observed experimentally. Another case consisting of nine stagnation points is shown in Figure 8(c). The central eddy rotates in the direction opposite to the tank, unlike the previous case.

CONCLUSION

Low Reynolds number flows in regions of complex geometry can be easily computed with the use of the boundary element method. Even in cases of complex flow patterns, quadratic source distributions along straight panels yield accurate results provided element lengths are optimized near re-entrant boundaries and corners.

ACKNOWLEDGEMENT

This work was supported by the Engineering Research Institute of Iowa State University.

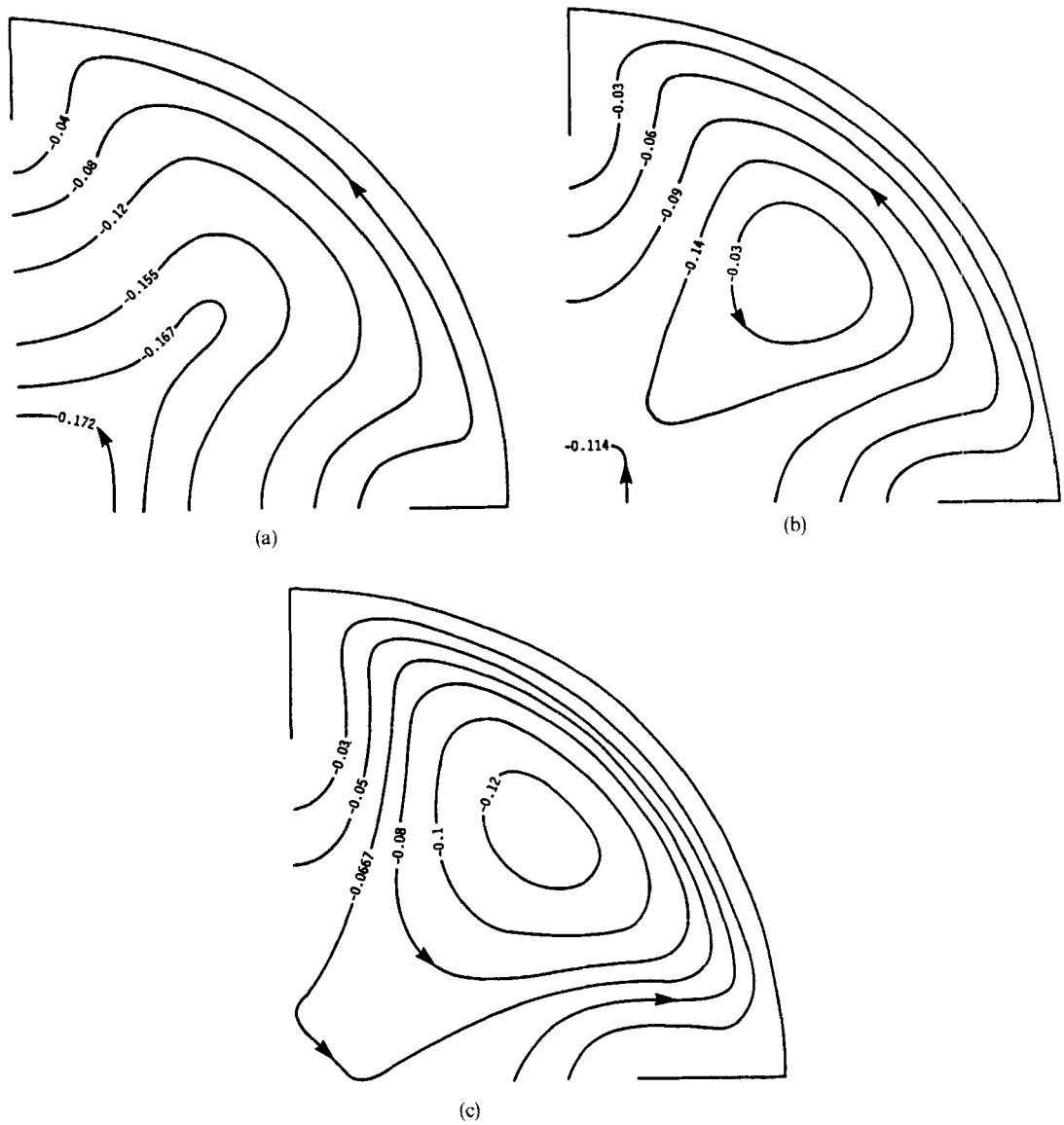

Figure 8. Streamline pattern for four barriers with (a) $h/D = 0{\cdot}2$, (b) $h/D = 0{\cdot}25$, (c) $h/D = 0{\cdot}3$

APPENDIX

The expressions for the integrals appearing in U_{kij} and V_{kij} are

$$\int_{\partial\Omega_j} \ln|\mathbf{p}-\mathbf{q}|\,ds(\mathbf{q}) = J_1,$$

$$\int_{\partial\Omega_j} \mathbf{q}\ln|\mathbf{p}-\mathbf{q}|\,ds(\mathbf{q}) = J_2 + a\cos\beta J_1,$$

$$\int_{\partial\Omega_j} \mathbf{q}^2 \ln|\mathbf{p}-\mathbf{q}|\,ds(\mathbf{q}) = J_3 + 2a\cos\beta J_2 + a^2\cos^2\beta J_1,$$

$$\int_{\partial\Omega_j} \frac{\partial}{\partial n}\ln|\mathbf{p}-\mathbf{q}|\,ds(\mathbf{q}) = [K_1 I_1 - K_2(I_2 + a\cos\beta I_1)]/a\sin\beta,$$

$$\int_{\partial\Omega_j} \mathbf{q}\frac{\partial}{\partial n}\ln|\mathbf{p}-\mathbf{q}|\,ds(\mathbf{q}) = [K_1(I_2 + a\cos\beta I_1) - K_2(I_3 + 2a\cos\beta I_2 + a^2\cos^2\beta I_1)]/a\sin\beta,$$

$$\int_{\partial\Omega_j} \mathbf{q}^2\frac{\partial}{\partial n}\ln|\mathbf{p}-\mathbf{q}|\,ds(\mathbf{q}) = \{K_1(I_3 + 2a\cos\beta I_2 + a^2\cos^2\beta I_1) - K_2[I_4 + 3a\cos\beta I_3 + a^2(4\cos^2\beta - 1)I_2 + a^3\cos^3\beta I_1]\}/a\sin\beta,$$

where

$$I_1 = \psi, \quad I_2 = a\sin\beta(\ln b - \ln a),$$

$$I_3 = a\sin\beta(h - a\psi\sin\beta), \quad I_4 = \tfrac{1}{2}a\sin\beta(b^2 - a^2),$$

$$J_1 = a\cos\beta(\ln a - \ln b) + h(\ln b - 1) + a\psi\sin\beta,$$

$$J_2 = \tfrac{1}{2}(b^2\ln b - a^2\ln a) - \tfrac{1}{4}(b^2 - a^2),$$

$$J_3 = \tfrac{1}{3}[(h - a\cos\beta)^3(\ln b - \tfrac{1}{3}) + a^3\cos^3\beta(\ln a - \tfrac{1}{3}) + a^2\sin^2\beta(h - a\psi\sin\beta)],$$

$$K_1 = a\sin(\alpha - \beta - \gamma), \quad K_2 = \sin(\alpha - \gamma).$$

The lengths a, b, h and the angles α, β, γ and ψ are shown in Figure 9. The field point $\mathbf{p}$ and source

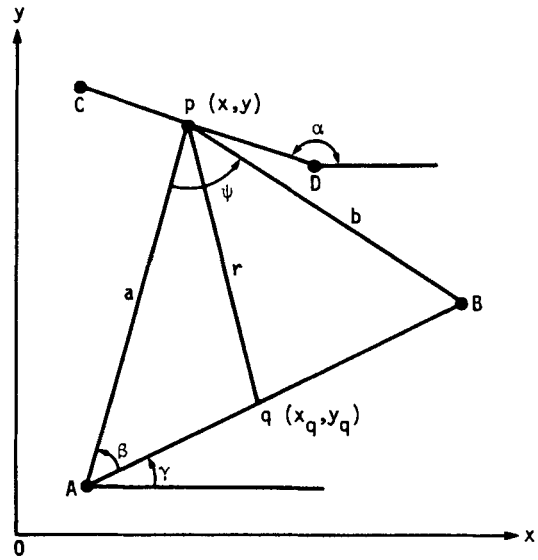

Figure 9. Evaluation of the integrals

point **q** are on the panels CD and AB respectively. No confusion between the angle ψ and the stream function should arise.

REFERENCES

1. M. A. Jaswon and G. T. Symm, *Integral Equation Methods in Potential Theory and Elastostatics*, Academic Press, London, 1977.
2. G. Fairweather, F. J. Rizzo, D. J. Shippy and Y. S. Wu, 'On the numerical solution of two-dimensional potential problems by an improved boundary integral equation method', *J. Comput. Phys.*, **31,** 96–112 (1979).
3. A. Mir-Mohamad-Sadegh and K. R. Rajagopal, 'The flow of a non-Newtonian fluid past projections and depressions', *J. Appl. Mech.*, **47,** 485–488 (1980).
4. M. A. Kelmanson, 'An integral equation method for the solution of singular slow flow problems', *J. Comput. Phys.*, **51,** 139–158 (1983).
5. M. A. Kelmanson, 'Modified integral equation solution of viscous flows near sharp corners', *Comput. Fluids*, **11,** 307–324 (1983).
6. M. J. M. Bernal and J. R. Whiteman, 'Numerical treatment of biharmonic boundary value problems with re-entrant boundaries', *Comput. J.*, **13,** 87–91 (1970).
7. I. Babuska and B. Szabo, 'On the rates of convergence of the finite element method', *Int. j. numer. methods eng.*, **18,** 323–361 (1982).
8. B. R. Munson and L. D. Sturges, 'Low Reynolds number flow in a rotating tank with barriers', *Phys. Fluids*, **26,** 1173–1176 (1983).
9. M. L. Schulock, 'The boundary integral equation method for the numerical solution of boundary value problems governed by second order elliptic systems', *Report TR-78-1184*, Air Force Office of Scientific Research, 1978.
10. D. B. Ingham, P. J. Heggs and M. Manzoor, 'The numerical solution of plane potential problems by improved boundary integral equation methods', *J. Comput. Phys.*, **42,** 77–98 (1981).
11. M. Vable, 'An algorithm based on the boundary element method for problems in engineering mechanics', *Int. j. numer. methods eng.*, **21,** 1625–1640 (1985).
12. M. S. Ingber and A. K. Mitra, 'Grid optimization for the boundary element method', *Int. j. numer. methods eng.*, **23,** 2121–2136 (1986).